Available online at www.sciencedirect.com
SCIENCE DIRECT
International Journal of Heat and Mass Transfer 49 (2006) 975–983
International Journal of HEAT and MASS TRANSFER
www.elsevier.com/locate/ijhmt

Modeling of trickle flow liquid fuel combustion in inert porous medium

Tarun K. Kayal *, Mithiles Chakravarty

Chemical Engineering Section, Central Glass and Ceramic Research Institute, Kolkata 700 032, India

Received 20 August 2004; received in revised form 9 September 2005
Available online 17 November 2005

Abstract

Present work is a numerical analysis of fuel oil combustion inside an inert porous medium where fuel oil flows through the porous medium under gravity wetting its solid wall with concurrent movement of liquid fuel and air under steady state conditions. A one-dimensional heat transfer model has been developed under steady state conditions using a single step global reaction mechanism. The effects of optical thickness, emissivity of medium, flame position and reaction enthalpy flux on radiation energy output efficiency as well as the temperature, position and thickness of vaporization zone have been presented using kerosene as fuel. Low values of optical thickness and emissivity of porous medium will ensure efficient combustion, maximize downstream radiative output with minimum upstream radiative loss.

Keywords: Liquid fuel combustion; Inert porous medium; Heat transfer; Radiation; Modeling

1. Introduction

Combustion of premixed gaseous fuel–air mixture inside the solid porous matrix releases energy to heat up the matrix which converts sensible heat of combustion to radiative energy. The radiative energy not only preheats the gas–air mixture for combustion augmentation but also emits radiation in the downstream end to heat up the load. The porous gas burners in comparison to conventional burners have higher thermal efficiency, higher power density (compact), low emission of CO and NO_x and better flame stability. Various thermal applications have been reported in last few decades utilizing these advantages [1,2].

Many analytical and experimental studies have been made to analyze the combustion characteristics of porous medium burner for premixed gaseous fuel–air mixture system [3–7]. But only a few experimental and numerical studies have been reported for combustion of liquid fuel using porous medium. Kaplan and Hall [8], Durst et al. [9] used premixed fuel oil sprayed droplets in air in place of gaseous fuel–air mixture and studied the effect of various parameters on stabilized combustion inside porous ceramic mixture. Howell et al. [10] measured the effects of porous matrix on reaction rates, flammability limits and flame stabilization, radiant output using single-stage and multi-stage gaseous burners. Tseng and Howell [11] have conducted both experimental and numerical studies of liquid heptane droplet vaporization and combustion of vapour–air mixture inside inert porous medium made of zirconia. The flashback and blow-off limits of combustion within the porous structure were determined. It was concluded that smaller droplet size (<25 μm) of heptane could be vaporized in the low temperature region before the flame front. Kayal and Chakravarty [12] presented numerical analysis of combustion of liquid fuel droplets suspended in air inside an inert porous media. The effects of absorption coefficient, emissivity of medium, flame position on radiative energy output efficiency and optimum oil droplet size at the entry, defined as the maximum size for complete vaporization before entering the combustion zone, have been studied. Fuse

* Corresponding author.
E-mail address: tarun@cgcri.res.in (T.K. Kayal).

0017-9310/$ - see front matter © 2005 Elsevier Ltd. All rights reserved.
doi:10.1016/j.ijheatmasstransfer.2005.09.012

Nomenclature

a	specific area, m^{-1}
A	pre-exponential factor in reaction rate, s^{-1}
c_p	average specific heat of gas stream at constant pressure, J kg^{-1} K^{-1}
d	diameter of each fiber, m
D	diffusion coefficient, m^2 s^{-1}
E	activation energy, J kg mol^{-1}
E^*	emissivity of inert solid medium
E'	downstream radiative efficiency, $q^*(L)/q'$
E''	total radiative efficiency, $[q^*(L) - q^*(0)]/q'$
f	equivalence ratio
g	acceleration due to gravity, m s^{-2}
h_{gl}	heat transfer coefficient between gas and liquid, W m^{-2} K^{-1}
h_{gs}	heat transfer coefficient between gas and solid, W m^{-2} K^{-1}
h_{sl}	heat transfer coefficient between solid and liquid, W m^{-2} K^{-1}
i	radiation intensity, W m^{-2}
i_b	black body intensity, W m^{-2}
k	average thermal conductivity, W m^{-1} K^{-1}
K_{gl}	mass transfer coefficient between gas and liquid, kg m^{-2} s^{-1}
l	dimensionless vaporization thickness, δ/L
L	porous layer length, m
L^*	optical thickness, αL
m	fuel oil flow rate, kg m^{-2} s^{-1}
M	average molecular weight, kg kg mol^{-1}
M_1, M_2, M_3	dimensionless quantities as in Eq. (18)
n	number of vertical fibers per unit cross-sectional area of medium, m^{-2}
n_f	fuel concentration, kg mol m^{-3}
n_{O_2}	oxygen concentration, kg mol m^{-3}
p	pressure, N m^{-2}
p_v	partial vapour pressure, N m^{-2}
q	radiative heat flux, W m^{-2}
q^*	net radiative heat flux, W m^{-2}
q'	reaction enthalpy flux, W m^{-2}
Q'	dimensionless reaction enthalpy flux, $q'/\sigma T_i^4$
R	universal gas constant, J kg mol^{-1} K^{-1}
s	scattering coefficient, m^{-1}
Sc	Schmidt number
t	thickness of oil film, m
T	temperature, K
T_{ad}	adiabatic flame temperature, K
T'	gas temperature (K) at vaporization zone at $x = x'$
T_A	autoignition temperature, K
T_A^*	dimensionless autoignition temperature, $(T_A - T_i)/T_i$
T^*	dimensionless gas temperature, $(T_g - T_i)/T_i$
$T^{*\prime}$	dimensionless vaporization temperature, $(T' - T_i)/T_i$
$T^{*\prime\prime}$	dimensionless peak gas temperature, T_m/T_{ad}
u	average axial velocity, m s^{-1}
u_L	laminar burning velocity of stoichiometric oil–air mixture, m s^{-1}
V^*	dimensionless burning velocity, u_3/u_L
x	axial coordinate, m
x^*	axial coordinate at flame plane, m
x'	axial coordinate at vaporization plane, m
x''	axial distance between vaporization plane and flame plane, $x^* - x'$
x'''	value of x where $T^* = 0.01$
X	dimensionless axial coordinate, x/L
X^*	dimensionless axial coordinate at flame plane, x^*/L
X''	dimensionless axial distance of vaporization plane from flame plane, x''/L
y	mass fraction of gaseous product

Greek symbols

α	absorption coefficient, m^{-1}
φ	porosity
ρ	average density, kg m^{-3}
λ	latent heat of vaporization of liquid, J kg^{-1}
δ	vaporization zone thickness, m
γ	kinematic viscosity, m^2 s^{-1}
σ	Stephan–Boltzmann constant, W m^{-2} K^{-4}

Superscripts

+	forward direction
−	backward direction

Subscripts

e	exit plane
f	flame plane
g	gas
i	inlet
l	liquid
m	maximum
o	liquid surfaces
s	solid
∞	bulk
1, 2, 3, 4	interfacial planes

et al. [13] used radiant energy of kerosene flame and furnace walls for penetration through porous ceramic plate to vaporize the oil from the oil container for continuous oil vaporization and sustenance of its stable combustion.

Takami et al. [14] studied the combustion behavior of kerosene when the oil was added drop wise at the top of the porous ceramic plate and ignited at the bottom surface. Jugjai et al. [15] developed a porous medium

burner where kerosene was supplied drop wise to the top surface of the burner and swirling combustion air was supplied at the lower side of the medium where the mixing of oil vapour and air occurred. Finally, combustion occurred inside the burner system. Effects of various parameters on the thermal performance of the burner were studied. Jugjai and Polmart [16] used a set up containing porous ceramic medium and packed bed with air mixing chamber in between them. Kerosene was added drop wise to the top of the ceramic matrix. Kerosene was vaporized while traveling through porous matrix and met the swirling air in combustion chamber. The packed bed was used in the downstream section to convert a portion of gas sensitive heat to radiation energy for emission. Temperature profile for both axial and radial position of the setup was measured and analyzed. Martynenco et al. [17] investigated, by numerical simulation, self-sustaining combustion of a gaseous mixture in inert porous medium with prior vaporization of liquid droplets. The heat transfer between solid, liquid and gaseous phases has been analyzed keeping into account the collision of oil droplets on the solid wall of the medium and effect of heat transfer coefficient between liquid and solid on the medium superheat.

The present study numerically investigates the thermal behavior of a liquid fuel combustion within a highly porous ceramic matrix. For this study, the liquid fuel is considered to be added in a drop wise fashion uniformly over the top surface of the matrix and allowed to trickle through the system. The air inlet is also at the same location, through the top of the matrix. In this system, the vaporization is assumed to be complete in the precombustion zone of the porous medium. The effects of various properties of medium and operating parameters on the vaporization zone and radiant output have been investigated in this study.

2. Mathematical analysis

2.1. Analytical model

The schematic diagram representing one-dimensional model under steady state conditions is shown in Fig. 1. Liquid (kerosene) fuel and air both uniformly distributed over top horizontal surface of inert porous medium of length L, flow vertically downward through the medium inside an adiabatic duct in x-direction. The air with mass velocity ρu along with liquid, both in laminar flow, enter medium ($x = 0$) at temperature T_i. Vaporization of liquid occurs at $x = x'$ over thickness δ and mixture of liquid vapour and air burns near the region at $x = x^*$ and flows out at $x = L$ at temperature T_e. The porous medium is divided into three regions where A, B and C represent precombustion, combustion and post-combustion regions respectively. The interfacing planes which are perpendicular to x-direction are separating the regions and designated by 1, 2, 3 and 4. The radiative heat fluxes in forward and backward directions in the porous medium are q^+ and q^- respectively.

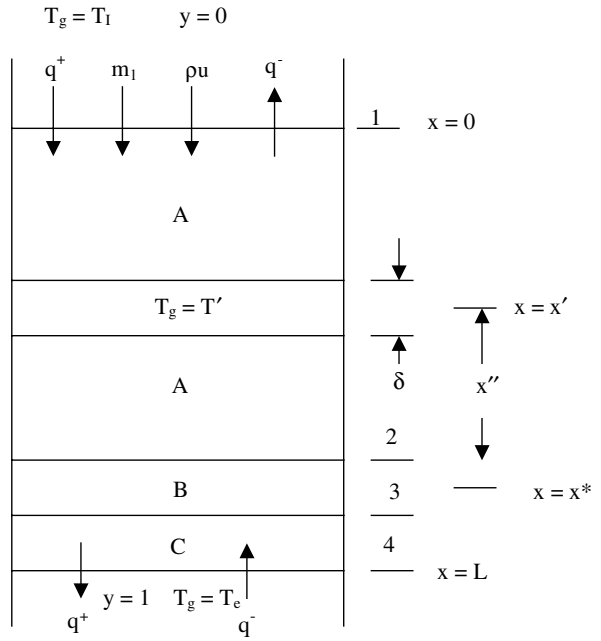

Fig. 1. Schematic diagram of liquid combustion system in a porous medium.

The principal assumptions used in the formulation are as follows:

(a) The working gas is non-radiating.
(b) The structure is having high porosity and the gas flow is laminar so that the pressure drop across the porous medium is negligible.
(c) The porous medium is a homogeneous continuum, the physical properties of which are given by multiplying those of porous material by a factor of $(1 - \varphi)$.
(d) The porous material is able to emit and absorb radiation in local thermal equilibrium while radiative scattering is ignored.
(e) A one-dimensional radiative propagation occurs in x-direction without any reaction occurring in regions A and C.
(f) The liquid film does not participate in radiative heat transfer within the medium.
(g) The heat transfer coefficient between solid and liquid, h_{sl} is estimated using a simplified flow structure inside the medium such as laminar flow of thin liquid film over the surface of a bundle of vertically stretched non-adhering thin fibers [18].
(h) The temperature of falling liquid film flowing over the solid surface of the medium is uniform over its thickness at any value of x.

The assumptions in the region B for reaction system are:

(i) The porous medium is non-catalytic.

(j) The liquid vapour–air mixture enters the region at a temperature $T_g \leqslant T_A$ where T_A is the autoignition temperature of liquid vapour–air mixture.
(k) The reaction starts and gets completed in the region at constant temperature $T_g = T_m$.
(l) The medium at interface 2 absorbs radiation as upward radiation flux in region A.
(m) The one-step global irreversible reaction between kerosene vapour and air is considered.

Some of these assumptions are discussed in detail. The assumption (a) is realized as the emissivity of the gas is much less than the porous solid medium. The assumption (b) is justified as the usual matrix structure of radiant burners [6] is in the form of ceramic porous open cellular foams or ceramic fiber structure which has very high porosity in the range of 0.95–0.99. Also low pressure drop across the porous solid is justified due to laminar flow of gas through these highly porous medium. The assumption (d) is justified to cover most of the porous medium such as ceramic foam [5] and porous metallic medium [19]. The assumption (e) is reasonable due to high thermal insulation outside the duct in presence of negligible radial flow. In the absence of published data for transmittance of transparent liquid kerosene ($C_{12}H_{26}$), the data [20] of transparent optical glass at 0.2–2 μ wave length may be used. For the maximum thickness of 18 μm (as is estimated in present study), the transmittance of glass is estimated [21] using Lambert's law as more than 99.9%. So the assumption (f) is justified because the radiation activity within the porous material between solid and gas will not be affected due to the presence of liquid adhering to the solid surface. The assumption (h) is realized as the value of Biot number ($h_{sl}t/k_l$) is estimated [22] as around 0.1.

The assumptions (j), (k) and (l) are discussed in totality. As the porosity of the solid medium is very high ($\varphi > 0.9$) and the mixture flow is laminar, the flow may be assumed to be of plug flow in nature. In kerosene–air combustion [23] the one-step global reaction rate is given by $k_c = 5 \times 10^{11} \exp[-30{,}000/RT_g][n_f]^{0.25}[n_{O_2}]^{1.5}$ g mol cm^{-3} s^{-1} when n_f and n_{O_2} are fuel and oxygen concentration in g mol cm^{-3} respectively using the composition of kerosene as $C_{12}H_{24}$. With reaction temperature of this system assumed at 2000 K and 99% completion of reaction under plug flow condition, the reaction thickness is estimated to be about a fraction of millimeter. This dimension is smaller or nearly equal to the dimension of cavity for highly porous ceramic [5] or metallic structure [19]. With high permeability and porosity of matrix structure, the combustion can be realized as if in open space flow condition in such a small thickness so that the assumption of constant temperature (T_m) of reaction temperature zone is justified as in assumption (k). The maximum temperature of the gas mixture before it enters the reaction region B is its autoignition temperature, T_A. However, the inlet temperature at interface 2 is determined by the absorptance of the porous medium facing reaction zone temperature, T_m. At steady state, the gas mixture at $T_g \leqslant T_A$ when enters the reaction region instantaneously reaches the reaction temperature T_m because of high reaction enthalpy flux. For methane combustion in porous matrix, the gas entry temperature, T_2 was obtained to be less than T_A [3]. So the assumption (l) is justified as the interface 2 exchanges radiative enthalpy from reaction region B only through emissive/absorptive interaction between reaction temperature T_m and low solid temperature at 2. Other assumptions (g), (i) and (m) are taken for computational simplicity.

2.2. Basic equations

Using above assumptions, the continuity equation for the species, energy equation for gas, liquid and solid phases are formulated respectively [4,24].

Region A

Prior to completion of vaporization ($0 \leqslant x < x' - 1/2\delta$),

$$\rho u c_p(\partial T_g/\partial x) = k_g(\partial^2 T_g/\partial x^2) - h_{gl}a_l(T_g - T_l) \quad (1)$$

$$\partial q^*/\partial x = k_s(\partial^2 T_s/\partial x^2) + h_{sl}a_l(T_s - T_l) \quad (2)$$

$$h_{gl}a_l(T_l - T_g) = h_{sl}a_l(T_s - T_l) \quad (3)$$

In vaporization zone,

$$h_{sl}a_l(T_s - T_l) = h_{gl}a_l(T_l - T_g) - \lambda(\partial m/\partial x) \quad (4)$$

Using wet bulb thermometry for air as non-condensable gas in the system [25],

$$h_{gl}a_l(T_l - T_g) = K_{gl}a_l\lambda(M_l/M_g)[p_{vo}/(p - p_{vo}) - p_{v\infty}/(p - p_{v\infty})] \quad (5)$$

$$h_{gl}/K_{gl} = 0.294[Sc]^{0.56} \quad (6)$$

For high mass ratio of air to fuel, $p_{v\infty} \approx 0$. The values of λ, p_{vo} and Sc are evaluated at T_l which is constant over the vaporization thickness $\Delta x = \delta$.

For fully developed laminar flow of falling film over n number vertical fibers of diameter 'd' under constant heat flux condition, h_{sl} is estimated [18] as

$$(h_{sl}/k_l)(\gamma^2/g)^{1/2} = 2.262[4m/(n\pi d\rho\gamma)]^{-1/2} \quad (7)$$

In post-vaporization zone, Eqs. (10) and (11) are used for the gas and solid phases.

Reaction region B

$$\rho u(\partial y/\partial x) = D\rho(\partial^2 y/\partial x^2) + A\rho(1 - y)\exp[-\{E/(RT_m)\}] \quad (8)$$

where mass production rate of species is in Arrhenius form

Equation of state: $\rho = Mp/(RT_g)$ (9)

Region C

$$\rho u c_p(\partial T_g/\partial x) = k_g(\partial^2 T_g/\partial x^2) - h_{gs}a_s(T_g - T_s) \quad (10)$$

$$\partial q^*/\partial x = k_s(\partial^2 T_s/\partial x^2) + h_{gs}a_s(T_g - T_s) \quad (11)$$

In region A and C, the net radiative heat flux, q^* is related to heat fluxes q^+ and q^- in forward and backward direction as

$$q^* = q^+ - q^- \tag{12}$$

Using two flux gray radiation approximation [24], the equation of transfer of intensity in each hemisphere is integrated over their respective hemispheres to yield forward and backward intensities i^+ and i^- as

$$\partial i^+/2\partial x = -(\alpha + s)i^+ + si^- + \alpha i_b \tag{13}$$

$$\partial i^-/2\partial x = -(\alpha + s)i^- + si^+ + \alpha i_b \tag{14}$$

where i_b is the black body intensity. As each intensity over their respective hemisphere is constant under the two-flux model, Eqs. (13) and (14) are integrated over each hemisphere to yield

$$\partial q^+/2\partial x = -(\alpha + s)q^+ + sq^- + \alpha\sigma T_s^4 \tag{15}$$

$$\partial q^-/2\partial x = -(\alpha + s)q^- + sq^+ + \alpha\sigma T_s^4 \tag{16}$$

At the interface 2, the absorptance of solid phase at temperature T_2 for incident blackbody radiation of reaction temperature T_m is equal to the emittance of surface at T_m for electrical non-conductors such as ceramics or metal oxide surfaces in which the monochromatic emittance is independent of temperature [20].

$$\text{At } x = x_2: \quad q^- = E^*\sigma T_m^4 - E^*\sigma T_s^4 \tag{17}$$

Other boundary conditions are

$$\begin{aligned} &x = 0: \quad T_g = T_i,\ q^+ = 0 \\ &x = x': \quad T_g = T' \\ &x = x_2 - \Delta x: \quad T_g \leqslant T_A \\ &\quad \Delta x \to 0 \\ &x = x_2: \quad y = 0,\ T_g = T_m \\ &x = x_3: \quad y = 1,\ T_g = T_m \\ &x = L: \quad T_g = T_e,\ q^- = 0 \end{aligned} \tag{18}$$

These equations are transformed into dimensionless form using following dimensionless equations:

$$\begin{aligned} &X^* = x^*/L, \quad T^* = (T_g - T_i)/T_i, \quad M_1 = \rho u c_p/(\sigma T_i^3) \\ &M_2 = k_s/(\sigma T_i^3 L), \quad M_3 = k_g/(\sigma T_i^3 L), \quad L^* = \alpha L \end{aligned} \tag{19}$$

The energy balance of the reaction zone B is worked out by considering the total reaction heat release rate, sensible enthalpy flux of gas and radiative energy flux at both ends of the zone. The overall energy balance of the system is made by equating the total reaction heat release rate to the sum of latent heat absorption loss, sensible enthalpy flux at downstream end, radiation heat losses at upstream and downstream ends. Heat conductivity energy fluxes at both ends of porous medium are assumed to be negligible [3].

2.3. Numerical solutions

The governing differential equations with boundary conditions were numerically integrated using collocation method [26]. In this method, the differential equations were converted to non-linear system of equations and solved with assumed polynomial spatial profiles for temperature and heat fluxes.

The computation was carried out using kerosene–air system in ceramic porous medium. Taking composition of kerosene as $C_{12}H_{26}$, the properties of $C_{12}H_{26}$ as function of temperature were used [23]. The autoignition of kerosene, $T_A = 503$ K was used. The adiabatic flame temperature, T_{ad} of $C_{12}H_{26}$ in air at $f = 1$ is taken [29] as 2277 K. The value of $h_{gl}a_l$ were estimated using long fibers of 100 μm diameter [27]. The value of h_{gl} is assumed to vary proportionately with $Re_g^{0.5}$ in laminar flow condition [18]. In estimating $h_{gs}a_s$, $d = 100$ μm was used [27]. For kerosene–air system, laminar burning velocity, u_L for $f = 1$ at 477 K is taken [28] as 0.40 m s^{-1}. The base line data are as follows:

$$\begin{aligned} &Q' = 1 \times 10^4, \quad T_i = 298\ \text{K}, \quad f = 1.0, \quad L = 0.1\ \text{m} \\ &\varphi = 0.95, \quad c_p = 1.105\ \text{kJ kg}^{-1}\ \text{K}^{-1}, \quad d = 100\ \mu\text{m} \\ &k_g = 0.078\ \text{W m}^{-1}\ \text{K}^{-1}, \quad k_s = 0.18\ \text{W m}^{-1}\ \text{K}^{-1} \\ &s = 0, \quad E^* = 0.3, \quad h_{gs}a_s = 2 \times 10^7\ \text{W m}^{-1}\ \text{K}^{-1} \end{aligned}$$

3. Results and discussion

The temperature of gas, liquid and solid coincide due to firstly, high value of $h_{gs}a_s$ imposed [4,5], secondly high value of h_{sl} and h_{gl} prior to start of vaporization ($0 \leqslant x \leqslant x' - 1/2\delta$) and thirdly, the negligible effect of small heat of absorption rate for vaporization of liquid in comparison to high value of radiative heat flux and sensible heat of gas in the vaporization zone ($x = x'$). With peak temperature remaining above 2000 K, the assumption of constant reaction temperature (T_m) is satisfied. In the post-vaporization zone, the air–fuel oil vapour mixture moves in region A so that the combustion of single phase occurs in region B. For combustion of single phase mixture containing by hydrocarbon and air at constant equivalence ratio f, flame can be stabilized [3,4,30] at any position of X inside the porous system.

Fig. 2 shows the gas temperature T^* profiles along the axial coordinate X inside the porous medium at different optical thicknesses L^* are shown with flame location $X^* = 0.5$. The absorption coefficient α of porous medium can be changed to vary L^* ($=\alpha L$) while L remains at 0.1 m. It is seen that the prereaction temperature zone length shortens significantly with increase in L^*. Here preheating temperature zone length $(x^* - x''')/L$ is defined arbitrarily as the dimensionless distance between $x = x^*$ and $x = x'''$ where $T^* = 0.01$ at $x = x'''$. However the interface solid temperature T_2 of the reaction zone B remains

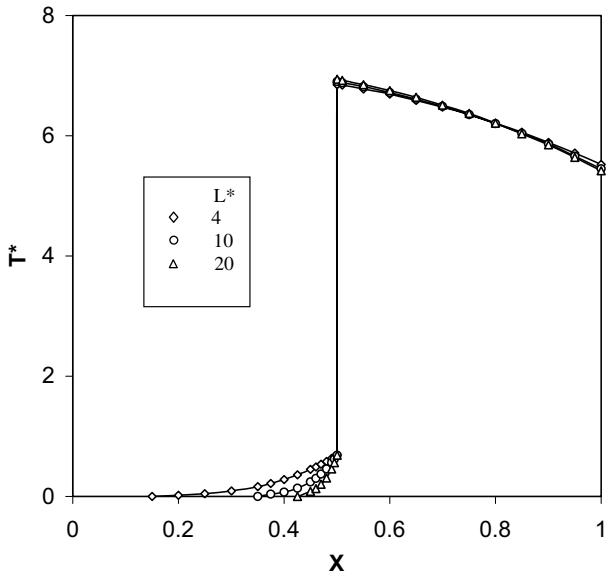

Fig. 2. Gas temperature profiles for several optical thicknesses when $X^* = 0.5$.

same at autoignition temperature ($T^*_A = 0.688$). Similar observations have been reported [4] for methane–air system.

Fig. 3 shows the effect of optical thickness L^* on the reaction peak temperature $T^{*\prime\prime}$, burning velocity V^*, vaporization temperature $T^{*\prime}$, thickness l, location X'' and radiative efficiencies E', E''. As L^* increases, the radiative energy feedback from the post-flame region to the reaction zone increases. But due to increase in L^*, the increase in the radiative energy feedback is partially neutralized with increase in radiative output at both downstream and upstream ends. These combined effect results in only marginal increase in $T^{*\prime\prime}$ and V^* with increase in L^*. However the reaction temperature is slightly greater than the adiabatic flame temperature i.e. $T^{*\prime\prime} \approx 1$ with increase in L^*. However, the reaction temperature is slightly greater than the adiabatic flame temperature i.e. $T^{*\prime\prime} \approx 1$. With increase in L^*, the combined effect of shortening of preheating temperature zone length and increasing of radiative heat flux in the region A results in increase in vaporization temperature $T^{*\prime}$ and decrease in vaporization thickness l and position X''. Pattern of decrease in l and X'' with increase in L^* is similar. It may be noted that the value of vaporization temperature $T^{*\prime}$ is much lower than the autoignition temperature T^*_A for the entire range of L^*.

Fig. 4 shows the radiative fluxes as a function of X in the porous medium when $X^* = 0.5$. Maximum radiative heat flux exchange occurs at the reaction zone $X^* = 0.5$. This supports the concept of radiative energy feedback in such system proposed by Weinberg [31]. At the reaction zone, there are sharp changes in forward and backward heat fluxes. At both ends of the porous medium, the net fluxes represent heat losses. Similar observations were made by others [3,24].

Fig. 5 shows the effect of position of reaction zone X^*, on gas temperature distribution. The reaction temperature $T^{*\prime\prime}$ and the interface solid temperature (T_2) do not significantly change in the range of $X^* = 0.2$–0.8 for $L^* = 10$. But in the preheating zone ($x < x^*$), its zone length, $(x^* - x''')/L$ increases and average temperature gradient, $\Delta T^*/\Delta X$ decreases with increase in X^*. These have significant effect on X'', $T^{*\prime}$ and l when X^* is varied.

Figs. 6–8 show the effect of variation of X^* on the position X'', the temperature $T^{*\prime}$ and thickness l of vaporization zone respectively and have been discussed together. At constant optical thickness L^*, the increase in X^* results in decrease in temperature gradient and increase in zone

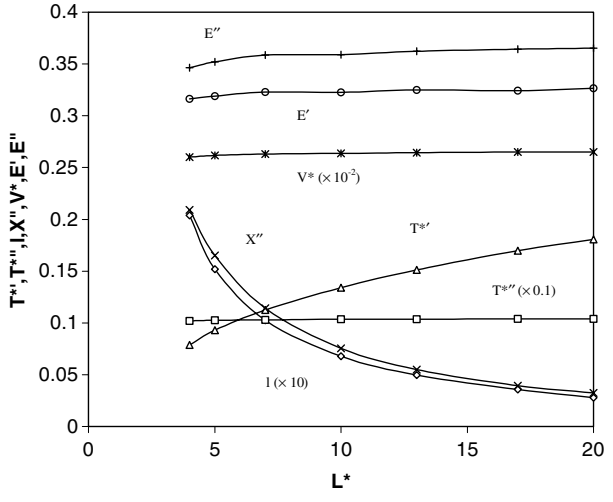

Fig. 3. Radiative output, peak gas temperature, burning velocity as well as temperature, position and thickness of vaporization zone for varying optical thicknesses at $X^* = 0.5$.

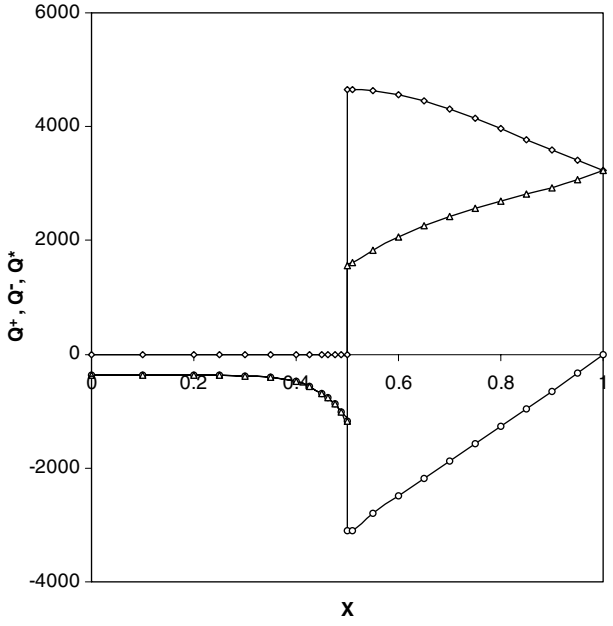

Fig. 4. Profiles in the radiant fluxes in the porous medium for $L^* = 10$, $X^* = 0.5$.

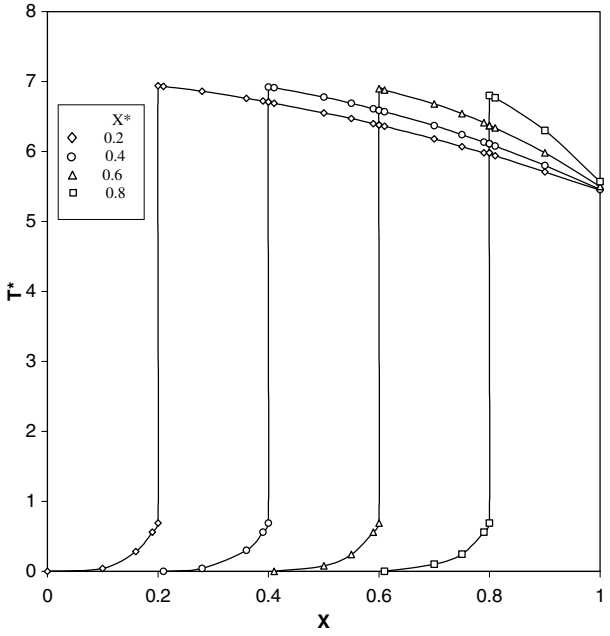

Fig. 5. Gas temperature profiles for several positions of the reaction zone for $L^* = 10$.

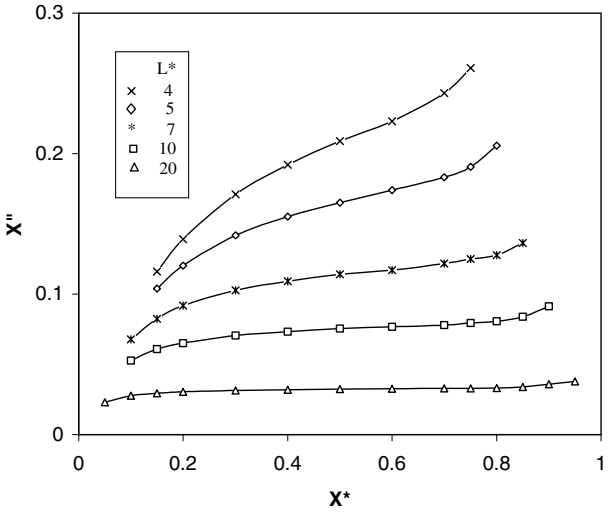

Fig. 6. Effect of position of reaction zone on the position of vaporization zone at various optical thicknesses.

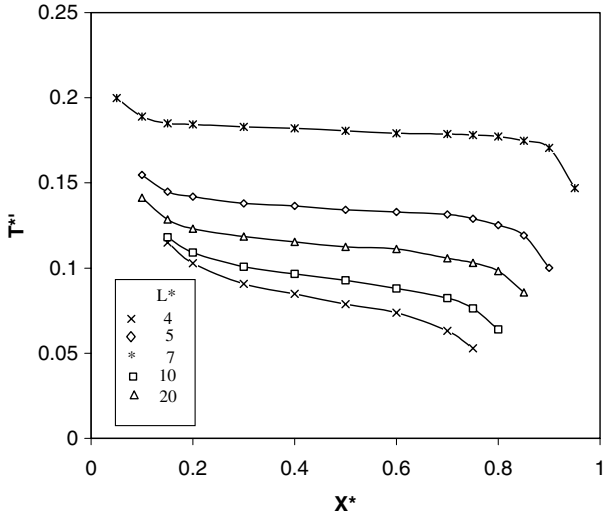

Fig. 7. Effect of position of reaction zone on the vaporization temperature at various optical thicknesses.

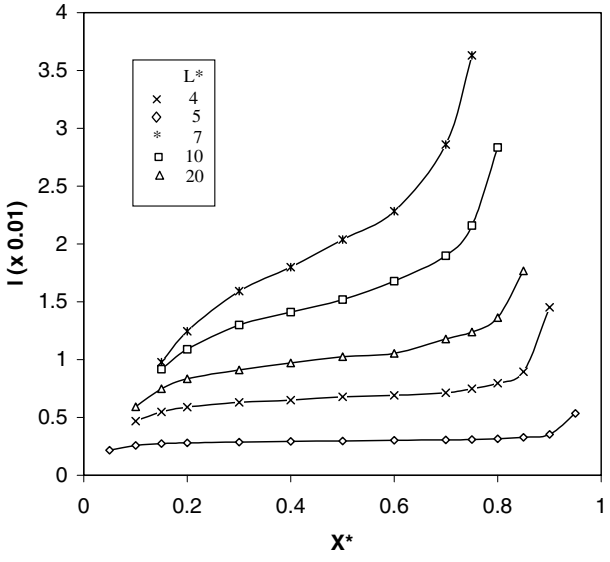

Fig. 8. Effect of position of reaction zone on the thickness of vaporization zone at various optical thicknesses.

thickness of preheating temperature zone (Fig. 5). Due to increase in preheating zone thickness, the vaporization position X'' increases but the vaporization temperature $T^{*\prime}$ decreases. Due to decrease in temperature gradient, the vaporization thickness l increases. At low values of optical thickness L^*, the effect of X^* on X'', l and $T^{*\prime}$ is prominent and noticeable as the preheating temperature zone is large (Fig. 2). At high values of L^*, the temperature gradient is so steep that the effect of X^* on X'', l and $T^{*\prime}$ is not noticeable.

Fig. 9 shows the effect of emissivity of medium, E^* on the thermal performance of the system. The effect of E^* and L^* are similar except that E^* affects only the performance of the prereaction zone, whereas L^* affects that of the whole medium. Accordingly, the effect of E^* on l, X'' and $T^{*\prime}$ has similar trend but in lesser degree of change. The increase in E^* results in increase and decrease in the upstream and downstream radiative heat loss respectively.

Fig. 10 shows the effect of reaction enthalpy flux, Q' on thermal performance of the system. Reaction temperature, $T^{*\prime\prime}$ and burning velocity, V^* increase almost linearly with Q'. But the values of X'' and l are nearly constant over the entire range of Q', which means that the vaporization activity is nearly unaffected.

Uniform oil vapour–air mixture should enter the combustion zone for efficient combustion of mixture. This will

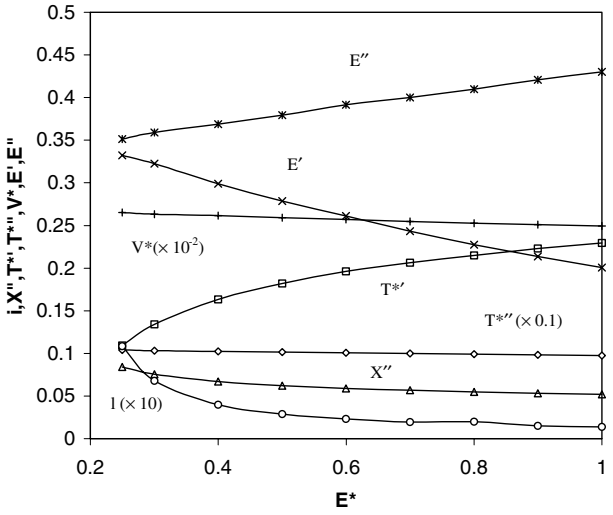

Fig. 9. Effect of emissivity of porous medium on radiative output, peak gas temperature, burning velocity as well as temperature, position and thickness of vaporization zone at $L^* = 10$, $X^* = 0.5$.

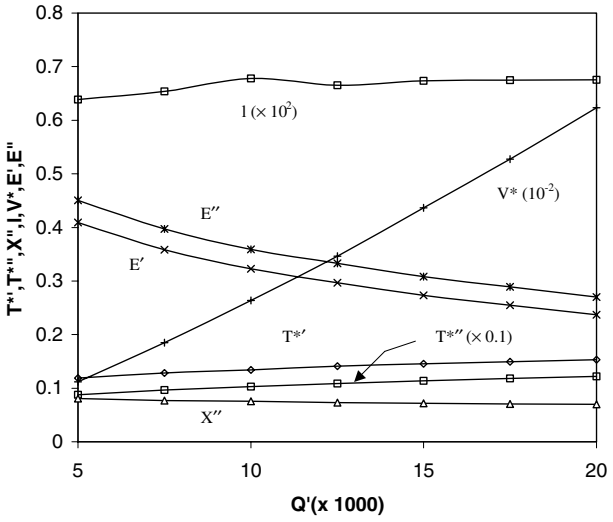

Fig. 10. Effect of reaction enthalpy flux radiative output, peak gas temperature, burning velocity as well as temperature, position and thickness of vaporization zone at $L^* = 10$, $X^* = 0.5$.

be ensured with high value of X'' i.e. high residence time of mixture in the post-vaporization zone prior to combustion. Low value of optical thickness of medium ($L^* \approx 4$–5) with flame position nearer to downstream end (i.e. $X^* > 0.5$) ensures high value of X''. Low values of absorption coefficient have been obtained using low pore density of medium [13]. In an industrial application, minimum upstream and maximum downstream radiative heat loss (for heating load) are desirable. This will be achieved for porous medium with low emissivity ($E^* \approx 0.25$). Usual material of construction of porous medium is Al_2O_3 or ZrO_2 which have low emissivity, E^* of 0.28 and 0.31, respectively at 2000 K [2].

4. Conclusion

A numerical investigation of combustion of fuel oil inside a porous medium has been presented where the liquid fuel falls under gravity in the form of a thin film on the wall of porous medium. Following are the conclusions of the investigation.

Firstly, low value of optical thickness of medium ensures efficient combustion due to high residence time in mixing of fuel oil vapour and air mixture in post-vaporization zone prior to combustion. Secondly, porous medium made of ceramic material with low emissivity is desirable for maximum downstream and minimum upstream radiative heat loss.

Acknowledgements

The authors express their sincere gratitude to Dr. H.S. Maiti, Director, CGCRI for his keen interest and encouragement in this work under the Institute project and kind permission to publish this paper.

References

[1] R. Echigo, Effective energy conversion method between gas enthalpy and gas radiation and application to industrial furnaces, in: Proceedings of the Seventh International Heat Transfer Conference, München, 1982, pp. 361–366.
[2] S. Mößbauer, O. Pickenäcker, K. Pickenäcker, D. Trimis, Application of porous burner technology in energy and heat engineering, in: Proceedings of the Fifth International Conference on Technologies and Combustion for a Clean Environment (Clean Air V), Lisbon, 1999, pp. 12–15.
[3] Y. Yoshizawa, K. Sasaki, R. Echigo, Analytical study of the structure of radiation controlled flame, Int. J. Heat Mass Transfer 31 (1988) 311–319.
[4] S.B. Sathe, R.E. Peck, T.W. Tong, A numerical analysis of heat transfer and combustion in porous radiant burners, Int. J. Heat Mass Transfer 33 (6) (1990) 1331–1338.
[5] P.F. Hsu, J.R. Howell, R.D. Mathews, A numerical investigation of premixed combustion within porous media, Trans. ASME, J. Heat Transfer 115 (1993) 744–750.
[6] D. Trimis, F. Durst, O. Pickenäcker, K. Pickenäcker, Porous medium combustion versus combustion systems with free flame, in: Proceedings of the Second International Symposium on Heat Transfer Enhancement and Energy Conservation, Guangzhou, China, 1997.
[7] A.J. Barra, J.L. Ellzey, Heat recirculation and heat transfer in porous burners, Combust. Flame 137 (2004) 230–241.
[8] M. Kapalan, M.J. Hall, The combustion of liquid fuels within a porous media radiant burner, Exp. Thermal Fluid Sci. 11 (1) (1995) 13–20.
[9] F. Durst, M. Keppler, M. Weclas, Air-assisted nozzle applied to very compact, ultra-low emission porous medium oil-burner, in: Proceedings of the Third Workshop (Spray 97), Lampoldshausen, 1997.
[10] J.R. Howell, M.J. Hall, J.L. Ellzey, Combustion of hydrocarbon fuels within porous inert media, Prog. Energy Combust. Sci. 22 (1996) 121–145.
[11] C.-J. Tseng, J.R. Howell, Combustion of liquid fuels in porous radiant burner, Combust. Sci. Technol. 112 (1996) 141–161.
[12] T.K. Kayal, M. Chakravarty, Combustion of liquid fuel inside inert porous media: an analytical approach, Int. J. Heat Mass Transfer 48 (2005) 331–339.

[13] T. Fuse, Y. Araki, K. Kobayashi, M. Hasatani, Combustion characteristics in oil-vaporizing sustained by radiant heat flux enhanced with higher porous ceramics, Fuel 82 (11) (2003) 1411–1417.
[14] H. Takami, T. Suzuki, Y. Itaya, M. Hasatani, Performance of flammability of kerosene and NO_x emission in porous burner, Fuel 77 (3) (1998) 165–171.
[15] S. Jugjai, N. Wongpanit, T. Laoketkan, S. Nokkaew, The combustion of liquid fuels using a porous medium, Exp. Thermal Fluid Sci. 26 (1) (2002) 15–23.
[16] S. Jugjai, N. Polmart, Enhancement of evaporation and combustion liquid fuels through porous media, Exp. Thermal Fluid Sci. 27 (8) (2003) 901–909.
[17] V.V. Martynenco, R. Echigo, H. Yoshida, Mathematical model of self-sustaining combustion in inert porous medium with phase change under complex heat transfer, Int. J. Heat Mass Transfer 41 (1) (1998) 117–126.
[18] S.M. Yih, Modelling heat and mass transport in falling liquid film, in: N.P. Cheremisinoff (Ed.), Handbook of Heat and Mass Transfer, Mass Transfer and Reactor Design, Vol. 2, Gulf Publishing Co., Houston, TX, 1986, p. 124.
[19] H. Yoshida, J.H. Yun, R. Echigo, T. Tomimura, Transient characteristics of combined conduction, convection and radiation heat transfer in porous media, Int. J. Heat Mass Transfer 33 (5) (1990) 847–857.
[20] E.R.G. Eckert, R.M. Drake, Analysis of Heat and Mass Transfer, McGraw-Hill, New York, 1972, p. 409, 599, 612.
[21] E.D. Olsen, Modern Optical Method of Analysis, McGraw-Hill, New York, 1975, p. 59.
[22] P.J. Schenider, Conduction, in: W.M. Rohsenow, J.P. Hartnett (Eds.), Handbook of Heat Transfer, McGraw-Hill, New York, 1973, pp. 3–37.
[23] G.L. Borman, K.W. Regland, Combustion Engineering, McGraw-Hill, New York, 1998, p. 323, 374, 570.
[24] S.W. Baek, The premixed flame in a radiatively active porous medium, Combust. Sci. Technol. 64 (1989) 277–287.
[25] R.E. Traybal, Mass Transfer Operations, McGraw-Hill, New York, 1955, p. 169.
[26] P. Razelos, Methods of obtaining approximate solutions, in: W.M. Rohsenow, J.P. Hartnett (Eds.), Handbook of Heat Transfer, McGraw-Hill, New York, 1973, pp. 4–72.
[27] T.W. Tong, S.B. Sathe, Heat transfer characteristics of porous radiant burners, Trans. ASME, J. Heat Transfer 113 (1991) 423–428.
[28] M.W. Thring, The Science of Flames and Furnaces, Chapman and Hall, London, 1962, p. 226.
[29] S.R. Turns, An Introduction to Combustion, McGraw-Hill, New York, 1996, p. 544.
[30] Y. Kotani, T. Tokeno, An experimental study on stability and combustion characteristics of excess enthalpy flame, in: The Nineteenth International Symposium on Combustion, The Combustion Institute, 1982, pp. 1503–1509.
[31] F.J. Weinberg, Combustion temperatures: the future, Nature 233 (5137) (1971) 239–241.